1959

X-ray detection of cladding effects

Herkner, Richard Thomas.; Pinkerton, Roy T.

Massachusetts Institute of Technology

X-RAY DETECTION OF CLADDING DEFECTS

RICHARD THOMAS HERKNER
AND
ROY T. PINKERTON

X-RAY DETECTION OF CLADDING DEFECTS

by

RICHARD THOMAS HERKNER

and

ROY "T" PINKERTON

SUBMITTED IN PARTIAL FULFILLMENT OF THE REQUIREMENTS FOR THE DEGREE OF NAVAL ENGINEER AND THE DEGREE OF MASTER OF SCIENCE IN NAVAL ARCHITECTURE AND MARINE ENGINEERING

at the

MASSACHUSETTS INSTITUTE OF TECHNOLOGY

May 1959

Signature of Authors .....

.....
Massachusetts Institute of Technology
May 25, 1959

Certified by .....
Thesis Supervisor

Accepted by .....
Chairman, Departmental Committee on Graduate Students

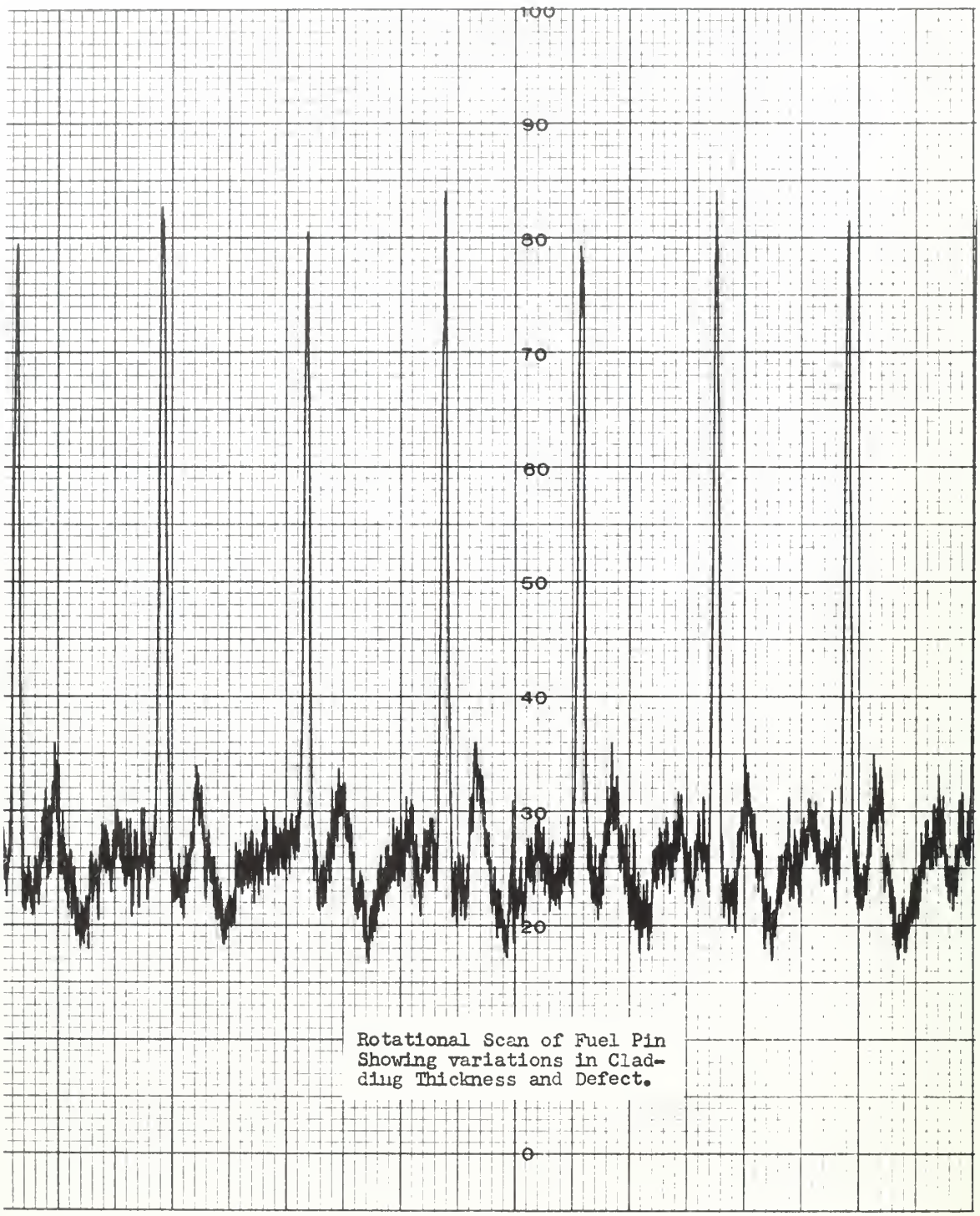

Rotational Scan of Fuel Pin Showing variations in Cladding Thickness and Defect.

X-RAY DETECTION OF CLADDING DEFECTS

by

RICHARD THOMAS HERKNER

and

ROY "T" PINKERTON

SUBMITTED TO THE DEPARTMENT OF NAVAL ARCHITECTURE AND MARINE ENGINEERING

ON MAY 25, 1959 IN PARTIAL FULFILLMENT OF THE REQUIREMENTS

FOR THE DEGREE OF NAVAL ENGINEER AND THE DEGREE OF MASTER OF SCIENCE

IN NAVAL ARCHITECTURE AND MARINE ENGINEERING

ABSTRACT

This thesis investigates the use of fluorescent x-ray attenuation as a non-destructive testing method for determining the thickness of zircalloy cladding on small diameter uranium fuel pins and the location of defects in this cladding. The initial investigation of the problem led to the choice of the uranium $L\alpha_1$ line as the one most suited for work in this field using standard commercially available x-ray equipment with x-ray tube voltages of 10 to 50 kilovolts. The investigation was conducted utilizing fuel pins 0.158 inches in diameter of the type that are to be used in the Enrico Fermi power reactor. These pins have a nominal cladding thickness of 6 mils. The results show that it is possible to measure cladding thickness accurately up to thicknesses of about 7 mils. The thinner the cladding, the more accurate is the measurement.

The results of the investigation to determine the feasibility of locating cladding defects showed that, while the equipment used located defects very well, the recording equipment did not allow the use of rotation speeds that would give a practical inspection time for the number of pins required in a core loading. By the use of suitable recording equipment and redesign of the present equipment to increase intensity, the method can be used. Success or failure for any particular inspection will depend on what type of defect is normally found in the pin and what standards the pin will be required to meet.

ACKNOWLEDGEMENTS

The authors would like to acknowledge their indebtedness to those who have aided in the preparation of this thesis: to the MIT Metallurgy Department for the generous loan of equipment; to R. Seger, instrument maker, for his aid in constructing the equipment; and to Nuclear Metals, Inc. for the provision of the sample fuel pins.

In particular we wish to express our thanks and gratitude to our thesis supervisor, Robert Olgivie, for his constant interest and advice.

TABLE OF CONTENTS

LIST OF TABLES

LIST OF FIGURES

GENERAL INTRODUCTION

Nondestructive testing techniques for thin zircalloy clad uranium fuel pins of small diameter are limited in number and have had little practical success in locating defects in the cladding on a production line basis. Although eddy current techniques have been applied for measuring the cladding thickness, the similarity in conductivity of the two metals is such that good results have not been obtained. The problem is very acute with small diameter fuel pins because of the desire to limit the volume ratio of the cladding to the fuel to acceptable limits and still safely contain the fissionable fuel and its fission products. Of other possible methods, autoradiography and beta ray attenuation are too time consuming and impracticable because of the large number of pins involved in each core.

A thesis by B. J. Lowe and P. D. Sierer at MIT in 1958 explored the possibility of using x-ray fluorescent techniques and Compton scattering as a means of measuring cladding thickness. The principle behind x-ray fluorescence is relatively simple. An x-ray machine is used to eject a K or L electron from the uranium atom. The filling of this vacancy by another orbital electron causes the emission of a characteristic K or L series x-ray, the line emitted being dependent on which particular electron fills the vacancy. The thickness of the cladding is then determined from the attenuation of these x-rays by the zircalloy cladding. This is expressed by the following equation:

$$I = I_o e^{-\mu x} \qquad (1)$$

where I_o is the initial intensity of the beam, I is the intensity of the

beam after having been attenuated by the thickness x of the cladding, and μ is the linear absorption coefficient of the cladding. The zircalloy cladding attenuates both the incoming beam and the outgoing radiation. Since the incoming beam is not a single wavelength but is a spectrum of wavelengths, μ is variable for the incoming beam. The spectrum changes with changes in tube voltage and current, so the equipment must be calibrated for any particular value of tube current and voltage. Although Sierer and Lowe measured cladding thickness of zirconium up to thicknesses of 30 mils, this was done with a 150 kv x-ray machine to excite the uranium K series. The attenuation coefficients for the K series lines of uranium are much lower than those for the L series. They were only able to measure thicknesses of 2 mils using the L series of uranium.[1] Their geometry was a limiting factor as well as the attenuation coefficient. Their thesis indicated that by use of better geometry and more intensity, it might be possible to measure thicknesses of zirconium (or zircalloy) up to 6 mils, but with decreasing accuracy for increased thickness.

This method of measuring cladding thickness also suggests a method of detecting cladding defects. Any defect in the cladding will have a lesser cladding thickness. X-rays passing through this area will not be attenuated to the same extent with a resultant higher counting rate.

To make use of this, a pure wavelength must be used. The L series from the fluoresced uranium would be lost in the intense K series of zirconium. Figure III shows relative intensities of the uranium and zirconium lines. By using a crystal spectrometer, a pure wavelength can be separated out from the rest of the spectrum. In this way, any L series line of uranium might be used.

Bragg's law is as follows:

$$n\lambda = 2 d \sin \theta \qquad (2)$$

where λ is the wavelength of the radiation, θ is the angle the ray makes with the crystal and d is the spacing between atomic planes in the crystal.

The ordinary flat crystal does not give very much intensity. The intensity of the line can be increased greatly by use of a bent crystal. The bent crystal focuses the desired wavelength into one area.[5]

The bent crystal geometry is shown in Figure 1. The crystal is bent to a radius of curvature that is twice the radius of curvature of the circle determined by the Source, Crystal (P) and the Detector. $1 = 2r \sin\theta$, d is the spacing between the planes in the crystal and λ is the desired wavelength. The radius that the crystal is bent to is R

$$R = \frac{1\ d}{\lambda}$$

FIGURE 1

BENT CRYSTAL GEOMETRY

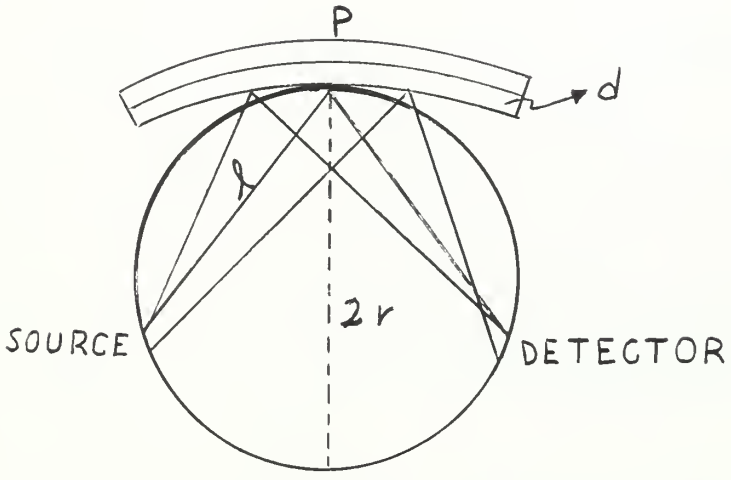

PRELIMINARY INVESTIGATION

An initial investigation was conducted to determine which line of the uranium L series would be best to use. Because of the lack of suitable data on the attenuation coefficients of zirconium, it was decided to measure the attenuation coefficient of zirconium for the wavelength region of interest.

Some of the factors to be considered in choosing the line were:

1. Intensity of the line.
2. X-ray target to give maximum intensity of the desired line.
3. Attenuation coefficient for the chosen line.
4. Resolution problems due to characteristic lines from cladding or alloying materials in the pin.
5. Type of crystal required to give maximum resolution for line chosen and which would be amenable for use in the bent crystal spectrometer.

This preliminary investigation was conducted using a standard Norelco x-ray fluorescent unit with a lithium fluoride crystal. A scan was made of the characteristic lines of zirconium and uranium to determine intensities and what resolution problems might be involved. These runs confirmed that:

1. The uranium $L\alpha_1$, $L\beta_1$, and $L\beta_2$ were of high enough intensity to justify their use over all other lines. A lesser possibility was the $L\gamma_6$.
2. Resolution problems would be encountered if the $L\beta_1$ or $L\beta_2$ were used due to the K series lines of the zirconium cladding and the molybdenum alloying agent used with the uranium.

Although the $L\beta_2$ has a higher initial intensity because of the x-ray tube used (Fig. III), its higher absorption coefficient makes its intensity decrease relatively quicker and it becomes less than that of the $L\beta_1$ for greater thicknesses of zirconium.

The same thing applies to the $L\alpha_1$ as compared to the $L\beta_1$ or $L\beta_2$ as it has a higher absorption coefficient than either of the other two. Consequently, although its original intensity is considerably more than the $L\beta_1$ or $L\beta_2$, it rapidly becomes less than either of these as the zirconium thickness is increased. This is actually an advantage rather than a disadvantage and the reasons therefore will be discussed later.

As Table I shows, the K series of both zirconium and molybdenum are of about the same wavelength as the $L\beta_1$ and $L\beta_2$. With a good crystal it would be possible to distinguish between these lines, but it will tend to increase the background* over what it would be if they were not so close in wavelength. (Fig. IV) Both the cladding and molybdenum would be fluoresced and emit their characteristic K series.

Figure V is the typical curve of spectrum intensity vs wavelength for an x-ray tube. The determining factor in the choice of the target in the x-ray tube was that a characteristic line of the target be of a slightly smaller wavelength than the L edge of the desired L series line. This gives the maximum intensity for the line. A molybdenum target fulfilled this criterion best and is easily obtained. The molybdenum K series characteristic line is just smaller in wavelength than the L_{III} edge of uranium which must be excited to obtain the $L\alpha_1$. (Table I)

* Background refers to general room background and scattered radiation unless otherwise noted.

It was decided that the L_{α_1} line offered the best possibility for success for the following reasons:

1. It has the highest initial intensity of the three possible lines.
2. Its absorption coefficient is relatively high, but not so high that all intensity is lost in a few mils of cladding.
3. No resolution problems encountered as there would be if either of the other two lines were used.
4. The high absorption coefficient allows the maximum differentiation in thickness in terms of counting rates.

TABLE I

Wavelengths of characteristic lines with applicable values of 2θ for a lithium fluoride crystal

	$K\alpha_2$	$K\alpha_1$	$K\beta_1$	$K\beta_2$
Zr	.791	.786	.701	.690
2θ	22.65	22.51	20.04	20.07
Mo	.713	.709	.632	.621
2θ	20.39	20.28	18.05	18.08
Ag	.564	.559	.497	.487
W	.213	.209	.184	.179

	$L\alpha_1$	$L\alpha_2$	$L\beta_1$	$L\beta_2$
U	.932	.911	.720	.755
2θ	26.54	26.14	20.59	21.61

TABLE II

Relative intensity of uranium L series lines

Line	Series	Relative Intensity	λ
$L\alpha_1$	L III	100	.932
$L\beta_1$	L II	80	.720
$L\beta_2$	L III	60	.755
$L\beta_3$	L I	30	.710
$L\beta_5$	L III	30	.726
$L\gamma_6$	L II	20	.595

FIGURE II

Intensity versus Wavelength for Uranium L Series using a Copper Target X-Ray Tube

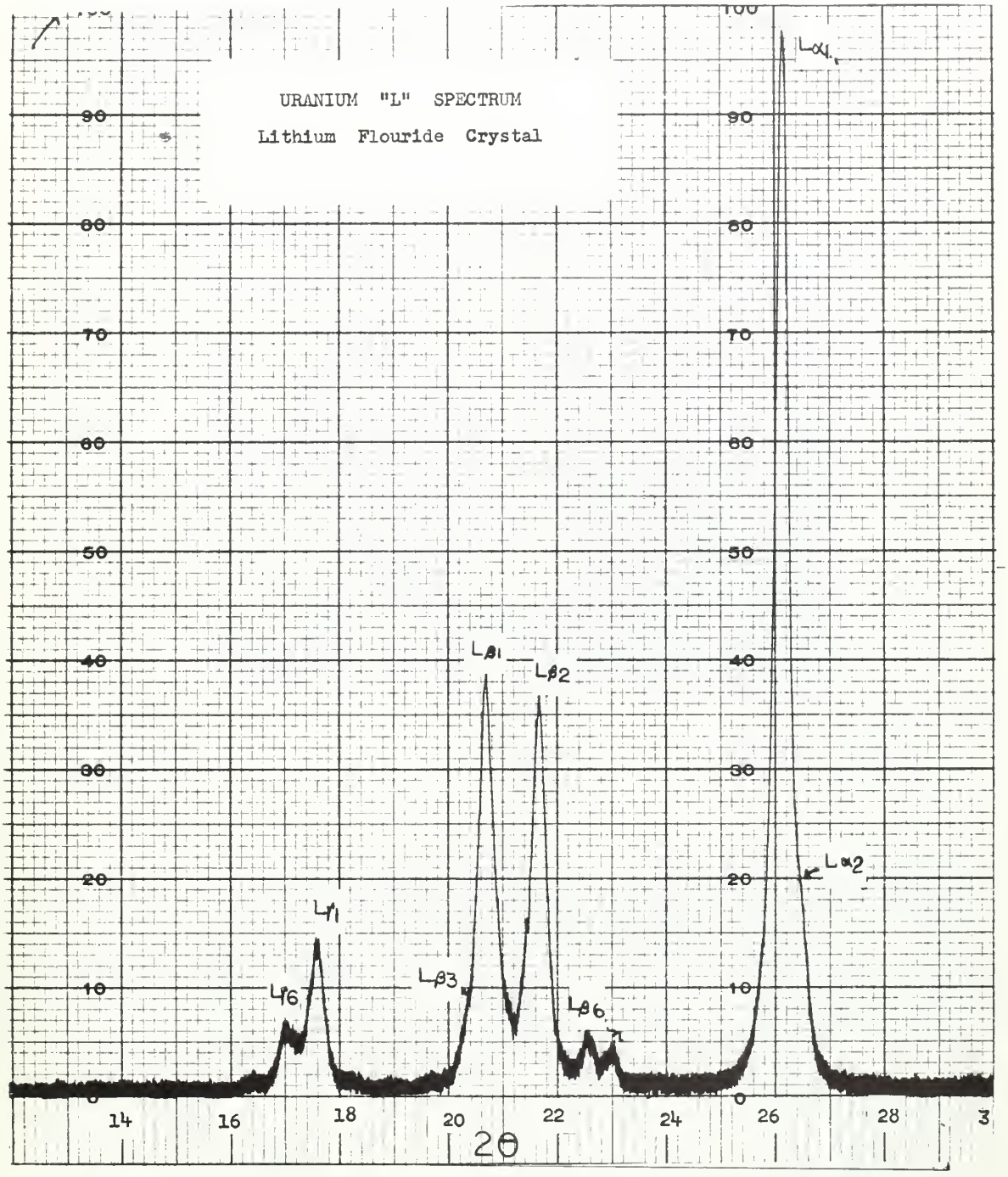

FIGURE III

Intensity versus Wavelength for Uranium L Series using a Molybdenum X-Ray Tube

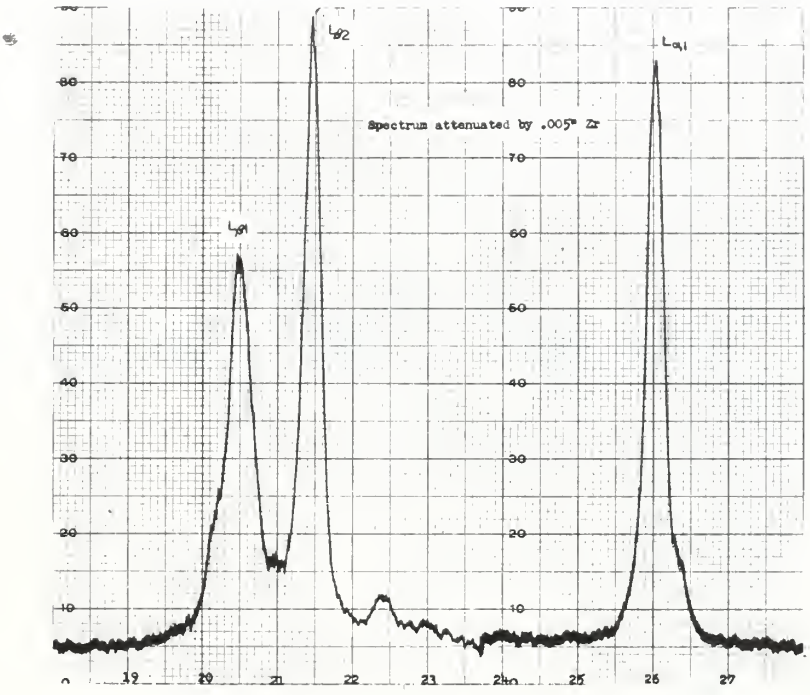

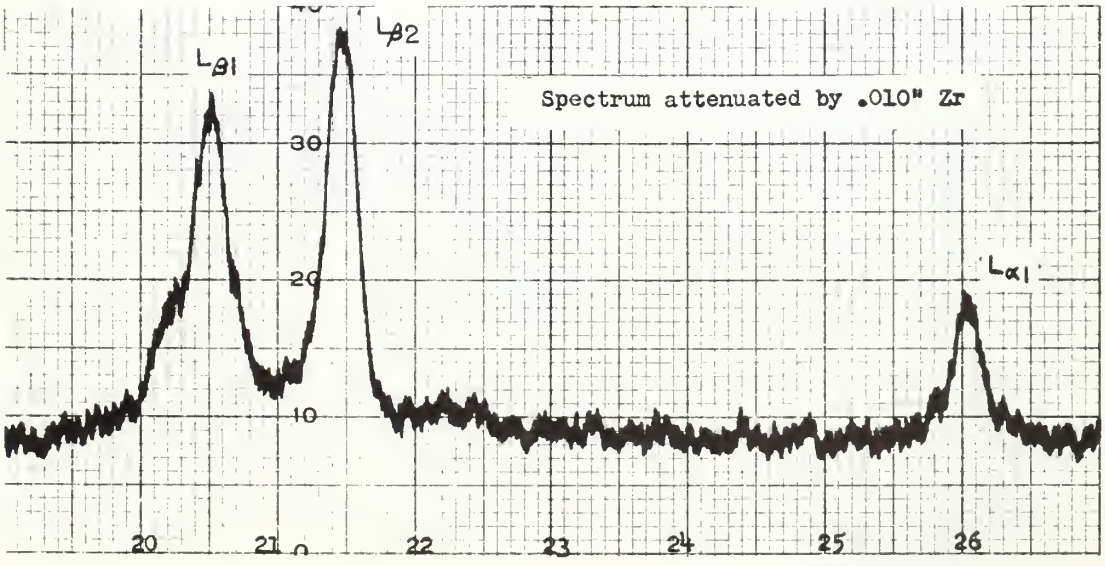

FIGURE IV

Intensity versus Wavelength of Characteristic lines from a Zircalloy Clad Uranium Fuel Pin

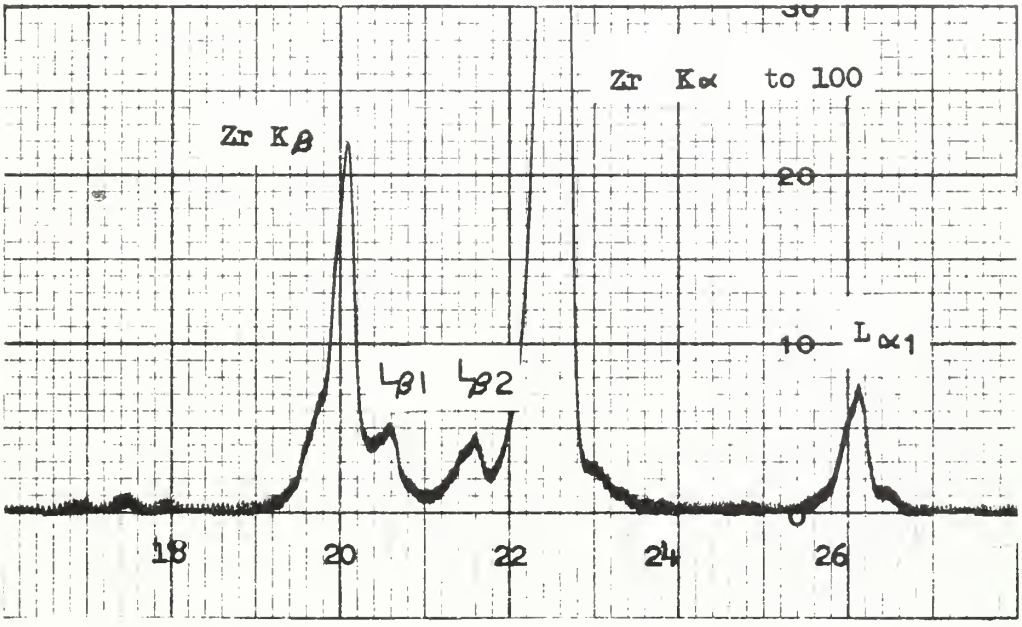

FIGURE V

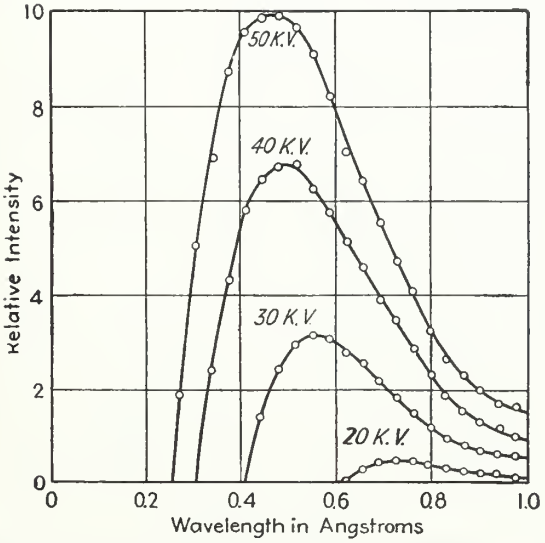

Distribution of energy in the continuous X-ray spectrum of tungsten at different voltages. (*Ulrey.*) (BARRETT)

FIGURE VI

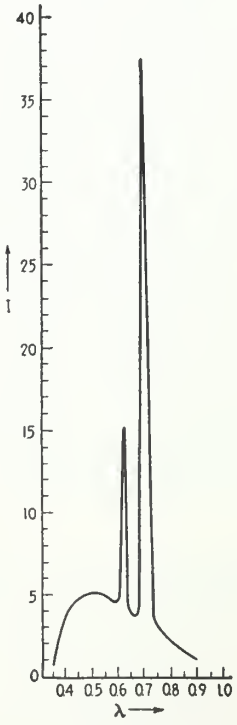

Spectrum of molybdenum at 35,000 volts showing $K\alpha$ and $K\beta$ lines superimposed on continuous spectrum. (BARRETT)

EQUIPMENT DESIGN

Once the initial investigation had been completed, the design of the equipment could be started. In essence, the equipment consists of an x-ray source, a foundation for the source, shielding against stray x-rays, a collimater to focus and control the size of the beam of x-rays striking the pin, a bent crystal to pick out the desired line and eliminate all other x-rays, and a detector for the x-rays. A standard Norelco OEG-50 molybdenum target x-ray tube was used as the x-ray source. The foundation and shielding consisted primarily of Alcoa tool and jig aluminum to reduce building time. Geometry, simplicity, and ease of construction were major factors in the design of the equipment.

The collimator (Fig. IX) is a brass block consisting of 2 pieces that allows the width of the beam to be varied by inserting shims between the two sections. To change the length of the beam, the collimator slit could be blocked by barium putty and thus allow only a portion of the slit to pass the x-rays. The collimator also acted as a major portion of the required shielding, since it is designed to fit snugly against the x-ray tube. The two pieces of the collimator fit together at an angle of 30^{o}.

The x-ray tube is supported by a built-up foundation. The head of the tube is housed in an aluminum box that acts as a secondary shield as well as a support for the bent crystal and detector.

Every effort was made to provide the best possible geometry while keeping construction simple. Thus the path lengths of 6" between specimen and crystal, and crystal and detector was determined to be the minimum practical distance for construction purpose. This also gave a practical radius for the bent crystal.

Although the $L\alpha_1$ was considered as the best line for the investigation and equipment design, consideration was also given to possible use of the other two lines. All that would have to be done would be to compute the radius of a bent crystal required for each line and make a new bent crystal for each line. A different x-ray target would be desirable for the $L\beta_1$ line, as it is not part of the L_{III} series lines.

The bent crystal structure consists of a brass piece machined to the proper radius and a lithium fluoride crystal bent to this radius. A set of thumbscrews allowed the crystal to be rotated around an axis parallel to the face of the crystal. The bent crystal could thus be "rocked" into the correct angular value for the desired line.

The detector was mounted on an arm which could be rotated around the same axis as the bent crystal. Another thumbscrew arrangement permitted small variations of the angle of the detector so it could also be "rocked" into the correct angle. A slit served as a detector window to allow only the beam from the $L\alpha_1$ line to be focused in the detector and cut out almost all other background radiation.

Two teflon pieces were used to provide bearing surfaces and act as a support for the pin. They also served to maintain a constant geometry while trial runs were being made. Lead sheet was used to line the inside of the aluminum box where survey meter readings indicated there was leakage of the x-ray beam. This was necessary because of the relatively low attenuation coefficient of aluminum.

FIGURE VII
Equipment Layout

FIGURE XI
X-Ray Tube, Pin and
Collimator

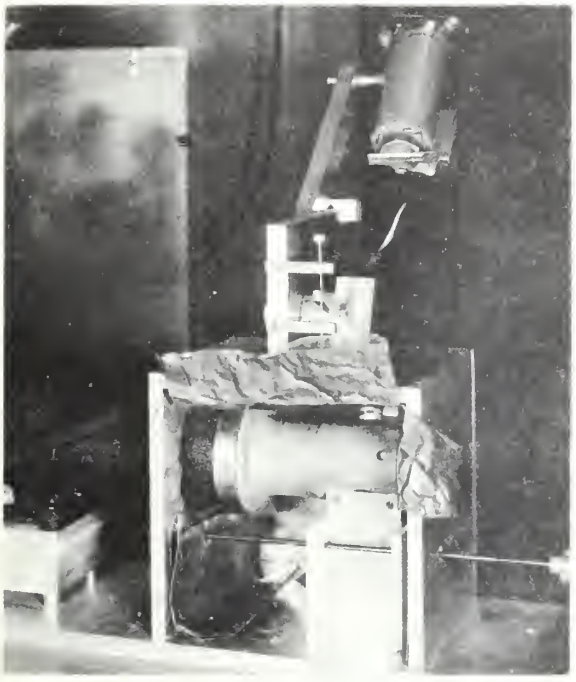

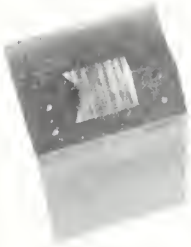

FIGURE IX
Collimator

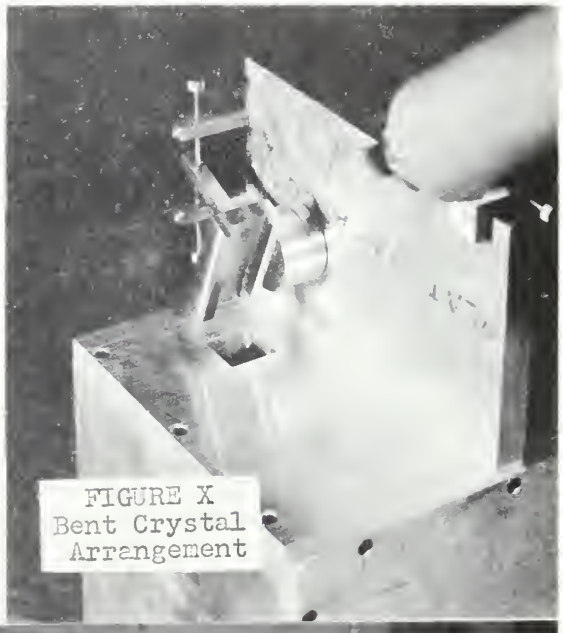

FIGURE X
Bent Crystal
Arrangement

FIGURE XII
Fuel Pins with Defects

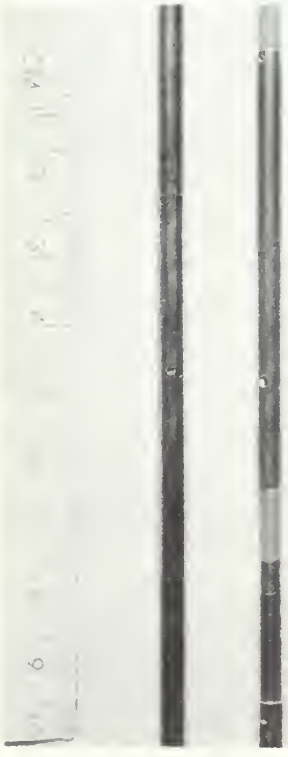

FIGURE VIII
Defect Detector
Equipment

FIGURE XIII

Schematic Arrangement of Defect Detector

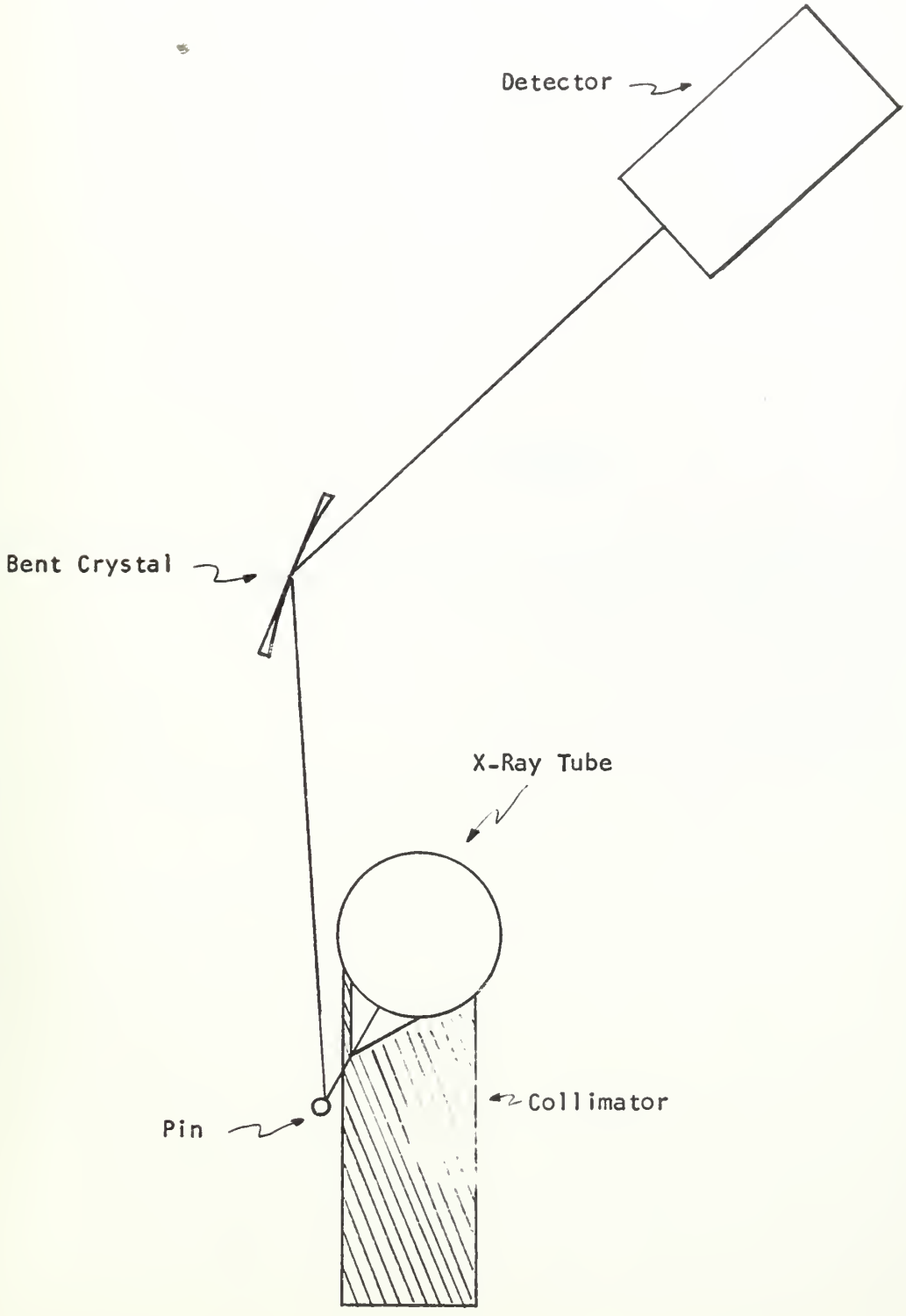

SECTION A

MEASUREMENT OF ZIRCONIUM ATTENUATION COEFFICIENT

PROCEDURE

The mass absorption coefficients for zirconium were measured by placing foils of known thickness in a beam of fluorescent x-rays and measuring the decrease in counting rate as compared to the original intensity. Fixed count time measurements were made. Wavelengths were obtained from the characteristic lines of known elements. An x-ray spectroscope was used to provide the pure wavelength separated out from the other wavelengths. Background was determined and subtracted out. Background was determined by rocking the detector off peak and measuring the counting rate.

The intensity (log) was plotted versus thickness and the slope of the curve found to determine the mass absorption coefficient for the particular wavelength. Since the data gave straight lines in practically all cases, no attempt was made to make a least squares fit to obtain the slope. The only point which in general did not fit on the straight line was the original intensity and this was due to the high counting rate causing the mechanical register to skip.

RESULTS

Table III

ELEMENT	LINE	WAVELENGTH	μ/ρ
Silver	$K\beta$	.497	40.2
Silver	$K\alpha$	.559	55.4
Molybdenum	$K\beta$	.632	74.1
Molybdenum	$K\beta$	.632	71.0
Niobium	$K\beta$	.665	89.6
Zirconium	K edge	.688	
Zirconium	$K\beta$	.701	15.0
Molybdenum	$K\alpha$	.710	15.4
Uranium	$L\beta 1$	.720	16.1
Yttrium	$K\beta$	.741	17.5
Niobium	$K\alpha$	.747	17.6
Uranium	$L\beta 2$	.755	18.5
Strontium	$K\beta$	.783	20.8
Zirconium	$K\alpha$	.786	20.4
Yttrium	$K\alpha$	.829	24.2
Lead	$L\gamma 1$	.840	26.4
Strontium	$K\alpha$	.875	28.0
Uranium	$L\alpha 1$	.911	31.1
Lead	$L\beta 1$	.982	38.7
Germanium	$K\beta$	1.129	56.7
Lead	$L\alpha 1$	1.175	64.4
Germanium	$K\alpha$	1.255	76.3

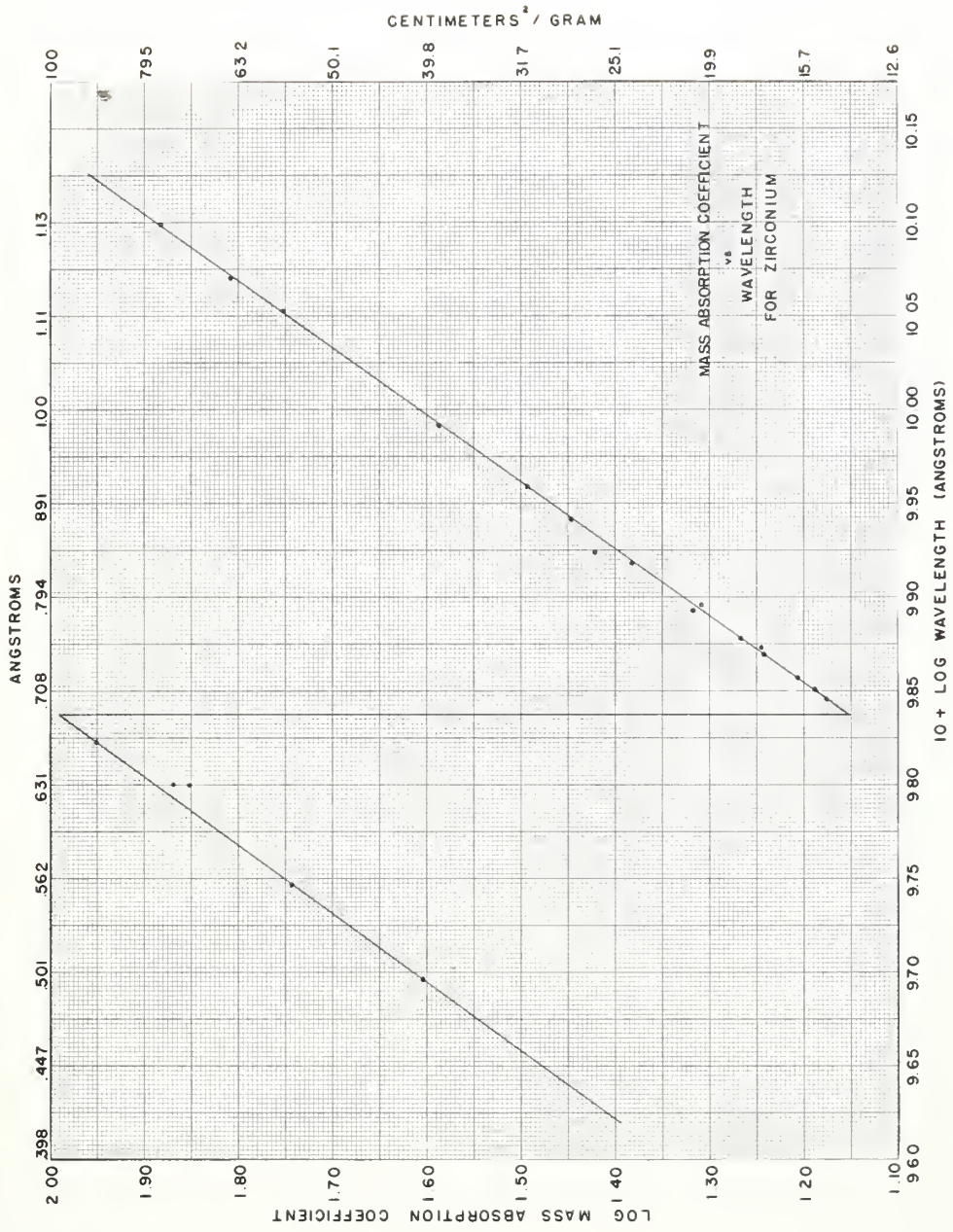

FIGURE XIV - ABSORPTION COEFFICIENT VERSUS WAVELENGTH

DISCUSSION OF RESULTS

As Figure XIV shows, the computed coefficients plot well as a straight line with the exception of two points, the molybdenum K_β and the lead $L_{\gamma 1}$. The slope of the line for wavelengths greater than the K edge is 2.99, as compared to the theoretical value of 3.0. The slope of the line for wavelengths less than the K edge is 2.56, which does not agree very well with the theoretical value. Since this wavelength region was outside the range of interest, the data was not rerun. Values for the mass absorption coefficient in this region would need further verification before use.

SECTION B

MEASUREMENT OF CLADDING THICKNESS
(Static Scan)

PROCEDURE

The investigation was conducted using a zircalloy clad uranium fuel pin with a nominal diameter of .158 mils. The instrument used is described under the equipment design section. Prior to any experimental work, the recording equipment was checked for normal operation as specified in the instruction manual. The zircalloy cladding was removed from a section of the pin to provide a uranium source which would provide a base counting rate for the cladding thickness measurements. Peak intensity was obtained by adjusting the crystal and detector to give a maximum counting rate from the uranium.

The effect of the following was investigated in this section of the thesis.

1. Effective collimator slit width and length
2. X-ray tube voltage and current
3. Detector window size
4. Geometry

The effect of the x-ray beam size, as determined by the collimator, was investigated using various widths and lengths to give a range of beam sizes that seemed desirable for detecting defects. Thin metal shims were used to vary the slit width from about 2.5 mils to 12 mils. The length was varied by blocking the slit with barium putty to give the desired length. Pictures were taken with film wrapped around the pin to determine the area of the beam striking the pin.

The effect of x-ray tube voltage and current was checked by making measurements with x-ray tube settings of 40 kv - 25 ma and 45 kv - 40 ma.

The size of the detector window was varied to see whether background could be reduced without reducing the peak intensity appreciably. Both length and width were varied. Pictures were taken of the beam entering the detector.

Changes in geometry were investigated by removing the teflon bearings and substituting a metal plate which placed the pin in the same position as did the teflon bearings, but permitted vertical movement of the pin. The change in counting rate as the pin was moved from its normal position was studied.

Fixed time count measurements were made with a fractional standard deviation ranging from .5% to .7% for the attenuation measurements and about 1.4% for background measurements.

The data was taken on a section of rod which was stripped of its zircalloy cladding. Foils could then be placed one by one around the pin to cover the uranium through which the beam passed to fluoresce the uranium. The foil was held in place on the pin by means of a clamp. After a series of measurements was obtained utilizing foils of one thickness, the background was obtained by rocking the crystal off peak and measuring the counting rate from the bare pin and after each additional foil was placed around the pin.

Three different thicknesses of foil were used to obtain the data.

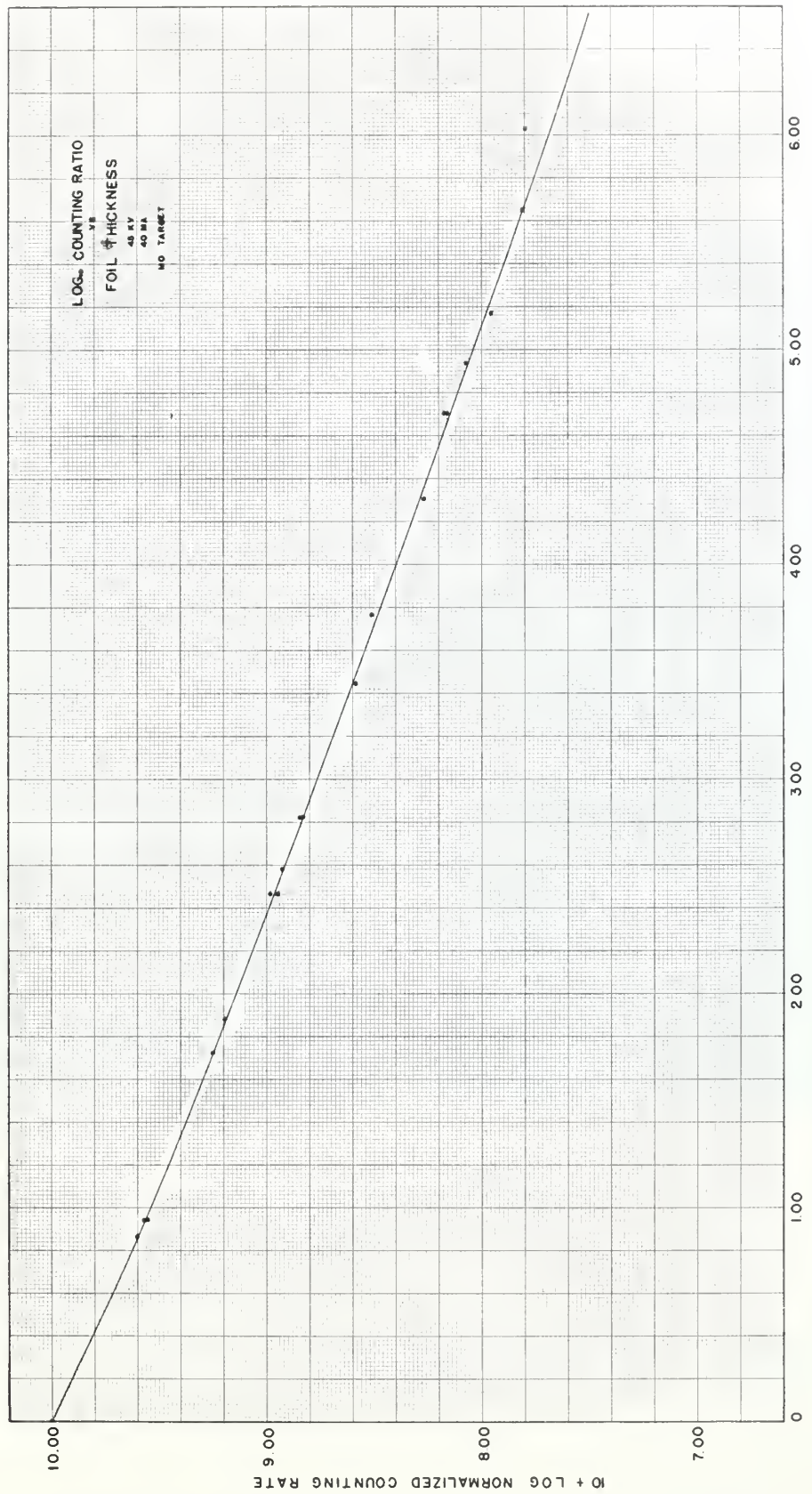

FIGURE XV - NORMALIZED COUNTING RATE VERSUS THICKNESS OF CLADDING WITH BACKGROUND EXCLUDED

FIGURE XVI

Normalized Counting Rate versus Thickness of Cladding for Different Tube Settings and with Background Included

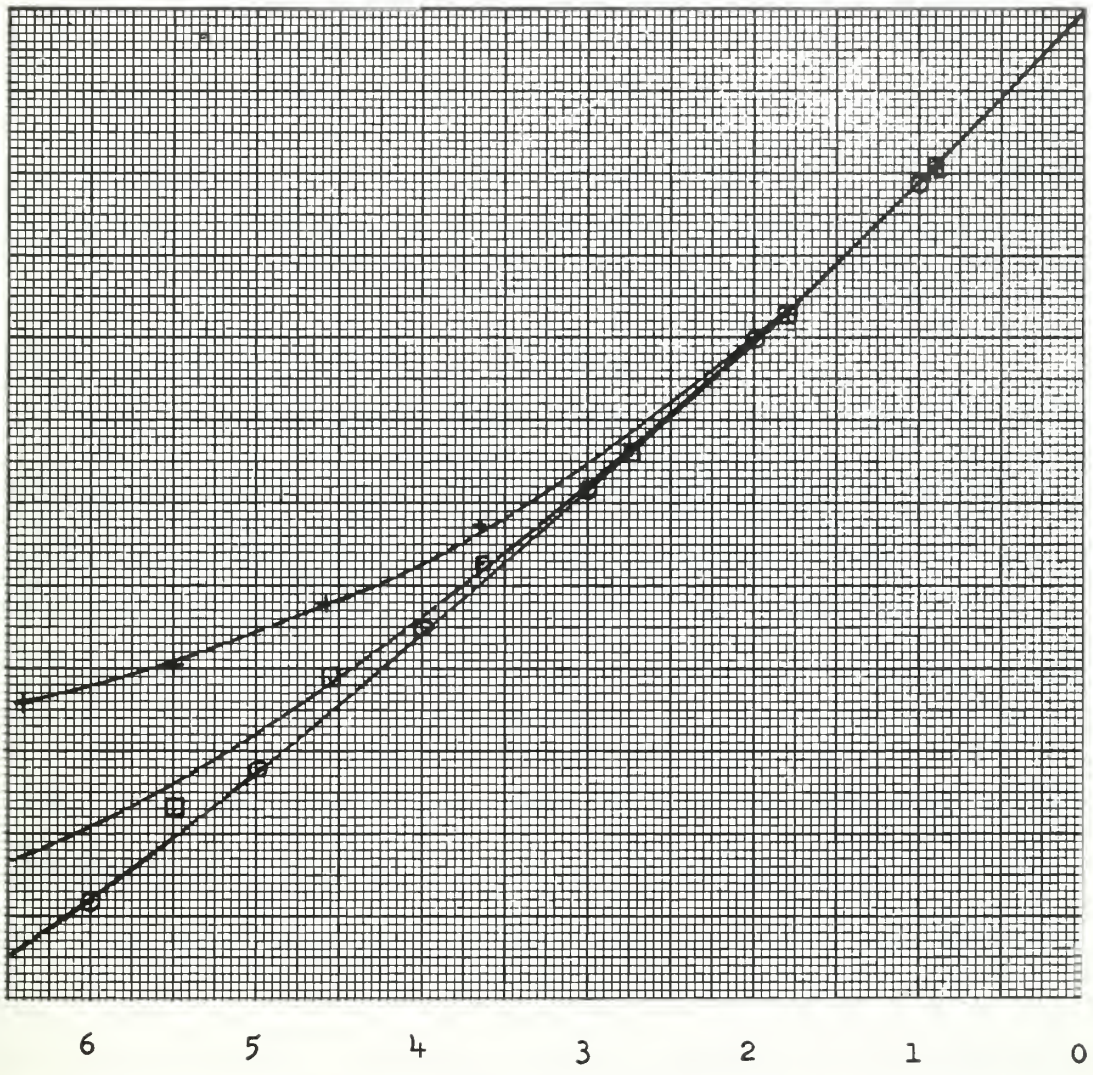

+ Tube Setting 40 kv 25 ma

⊙ Tube Setting 45 kv 40 ma

⊡ Tube Setting 45 kv 40 ma Noticeable change in background

DISCUSSION

The results clearly indicate that it is possible to measure the cladding thickness of small diameter fuel pins with good precision and accuracy up to about 7 mils of cladding thickness. The precision could be increased by increasing the total number of counts, but this is of little importance in a production process. Of the three different foil thicknesses used, any one could be considered to establish a calibration curve and the other two used as checks on the accuracy of the process by using the normalized counting rates obtained when using them.

There is little effect from a change in the collimator slit length or width as the points plotted consisted of data taken from smooth foils of constant thickness. However, for measurements made over fuel pins, the effect of slit size would be very strong. The type of defect would determine the desirable slit size and is discussed in the next section.

The effects of changes in tube voltage and/or current were not good. It was hoped that a normalized curve would be obtained which could be used independent of tube voltage or current if background was eliminated. This is not the case. A calibration curve can be made for any particular setting of the current and voltage and will be good for a small change, of the order of 1 ma or 1 kv, but it will not be good for large changes (Fig. XV). This is because the incoming beam is attenuated also. The wavelengths composing the incoming beam are attenuated differently, thus changing the spectrum, which in turn changes the intensity of the outgoing line. Thus the I_o changes as the thickness is varied. In addition to this effect, the spectrum is also changed by the changes in voltage (Fig. VI). The short wavelength cutoff constantly decreases as the tube voltage is

increasing, so that the spectrum reaching the uranium is different for each voltage and there is no way to determine the original intensity of the line.

Changing the detector window size caused background to become less. The beam reaching the detector from the pin was very narrow and long. Only a small window width was needed at the detector to permit the full line intensity to reach the detector. Any increase in size only increased background without appreciably increasing the main peak count. This is investigated more completely in Section C. Slit length was important, though. The length of the beam reaching the detector was larger than the detector crystal, so that some of the peak was lost. The slit used must be as long as the detector would permit or there is a loss of some of the intensity of the source. A doubly bent crystal would have been useful so that more of the intensity from the pin could have been used.

A bare uranium section of the pin, wrapped with foil to the desired thickness, was placed on the metal plate that replaced the teflon bearings. The metal plate permitted vertical movement of the pin. Although every effort was made to keep the pin aligned, it was impossible to get consistent results due to small movements of the rod from its normal position as fixed by the teflon bearings, showing that the geometry is somewhat critical.

It had been intended to use the above method to avoid having to turn the x-rays off each time another foil was added to the pin. A large section of foil was wrapped around the bare pin in such a manner that there were half inch sections with 1, 2, or 3, etc., foil thicknesses up to a thickness of six mils along the pin. Then it would have been necessary only to move the pin in and out of the instrument to make the measurement for each

thickness. Unavoidable small bumps in this foil wrapping caused the pin to have small vertical displacements and thus not give consistent results using the metal plate. These same defects prevented use of the teflon bearings, since the tight fit of the teflon did not permit free movement of the pin through the bearing. This necessitated turning off the x-ray machine each time a new foil was added and thus created some error from trying to obtain the same tube voltage and current and in not allowing sufficient time for the equipment to warm up.

It was found that the background was independent of the number of foils around the pin. There was a significant difference in background between the bare pin and the foil wrapped pin. If background could be depended on to remain constant, a calibration curve could be plotted including background. Normally it varies quite a bit and this would create a large error at the larger cladding thicknesses. The calibration curve must then be drawn with background taken out, and when being used, the measured values must also have the background subtracted. This effect is critical with thicknesses of cladding greater than 4 mils. (Fig. XVI).

SECTION C

CLADDING INSPECTION

PROCEDURE

The procedure followed here was similar to that used in measuring the cladding thickness in section B. A variable speed motor was used to rotate the pin. Rotation speeds of .7 rpm to 16 rpm were used. A suitable defect was placed on the pin and the pin rotated through the x-ray beam to investigate the effect of various conditions on the defect counting rate. Data for the rotating pin was taken with a Brown recorder. Fixed count time measurements were taken with the defect stationary in the beam for comparison with the rotation values and for calculations. X-ray photographs were taken of the beam at the pin, and at the collimator exit to find the effective area of the beam.

The following important aspects in the detection of cladding defects were investigated.

1. Types of defects - four types of defects were used. Holes of various sizes were drilled in the cladding. The cladding thickness was reduced by filing it down. Indentations were placed in the cladding by means of a Rockwell hardness testing machine. Foils with holes in them were wrapped around a section of the pin from which the cladding had been removed.
2. Speed of rotation - the pin was rotated at various speeds to determine what effect this would have on the counting rate of the defect.
3. Effect of length and width of collimator slit, i.e., x-ray beam area - assorted slit sizes were used to check the effect of length and width. Barium putty was used to control the length and shims were used to vary the width. The beam area was found from x-ray photographs.

4. Effect of window width at the detector - openings of different sizes were placed in front of the scintillation crystal to reduce background as much as possible.
5. Location of defect in beam - the defect was moved along the length of the beam to see if there was any variation in counting rate.

RESULTS

TABLE IV

Effect of Window Width at Detector

	Window Width	CPS	FSD
Defect Peaked	.375	498.0	.7%
	.025	325.8	.7%
Off Peak	.375	64.2	2.0%
	.025	20.4	2.0%

Window Width

.375" $\frac{\text{Peak}}{\text{Background}}$ $\frac{498.0}{64.2} = 7.76$

.025 $\frac{\text{Peak}}{\text{Background}}$ $\frac{325.8}{20.4} = 15.97$

FIGURE XVII

Defect Peaks for Different Window Width at Detector

(Also Effect of Change of Scale)

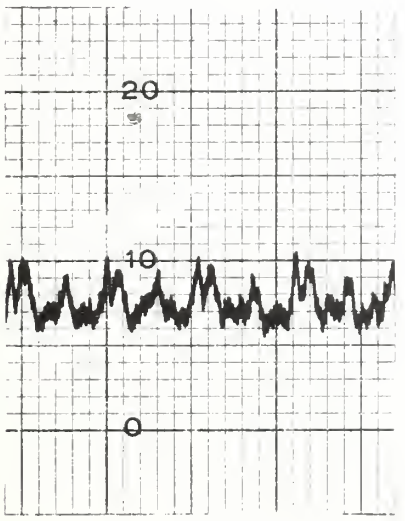

a.

Window Width .025 " SF=16cps

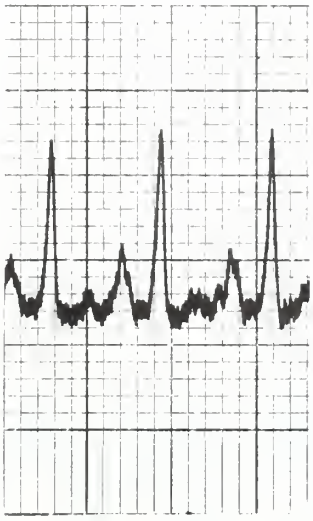

b.

Window Width .375 " SF=8cps

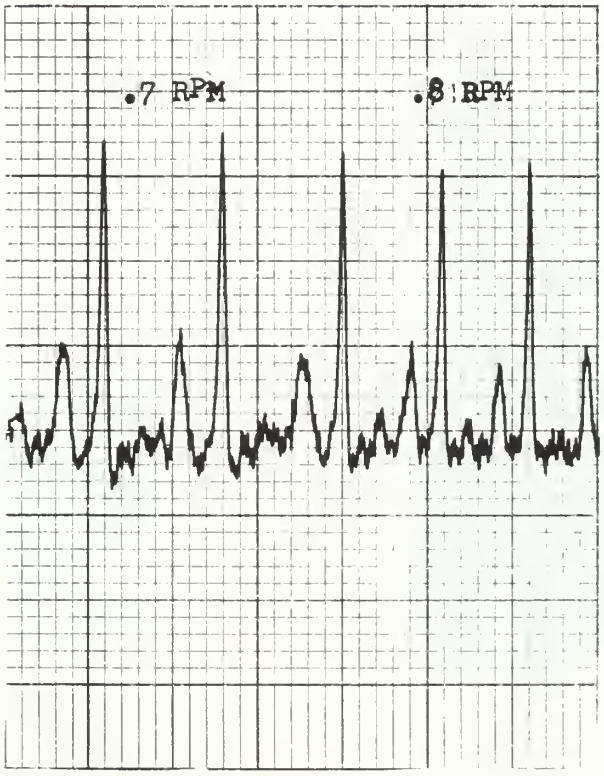

c.

Window Width .375" SF=8cps

FIGURE XVIII
Defect Peaks for Various Rotation Speeds and Time Constants

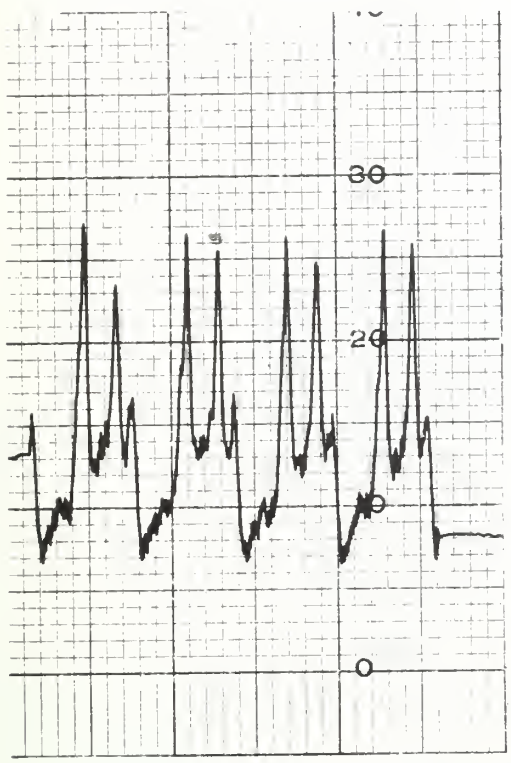

a.

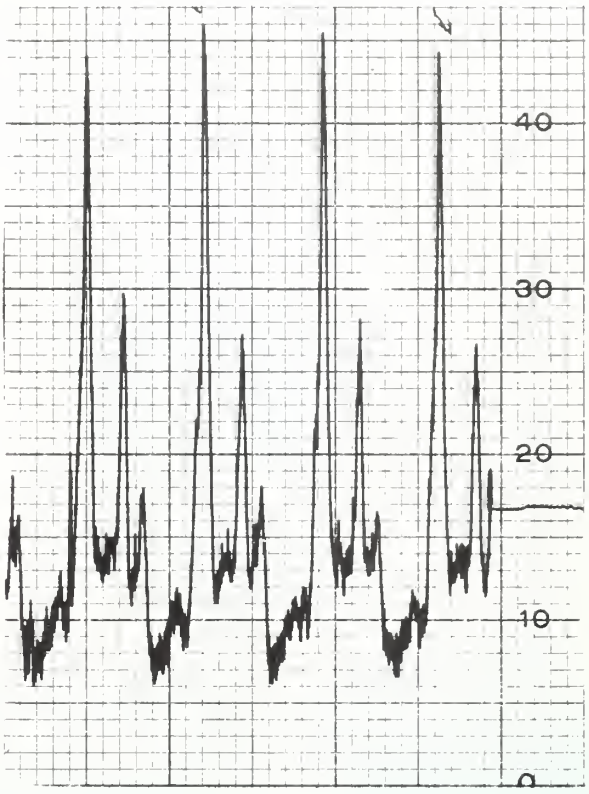

b.

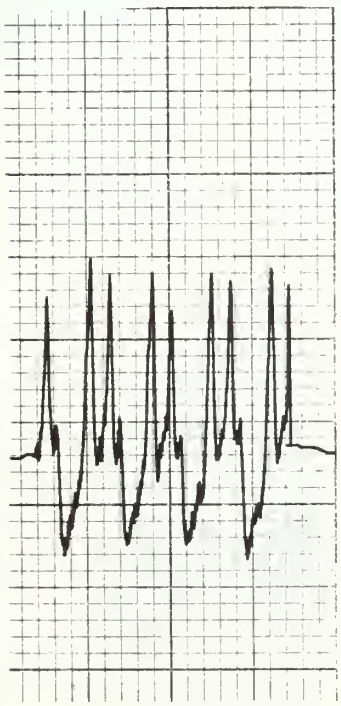

c.

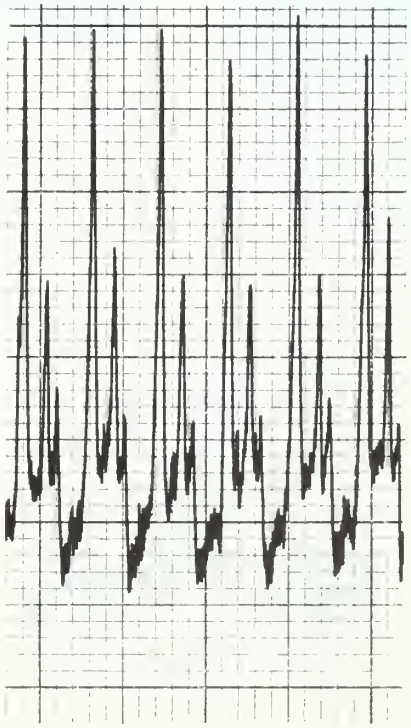

d.

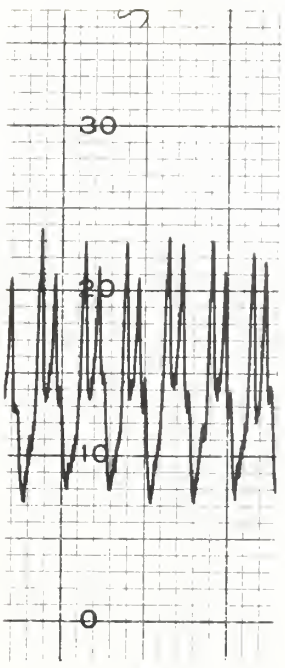

e.

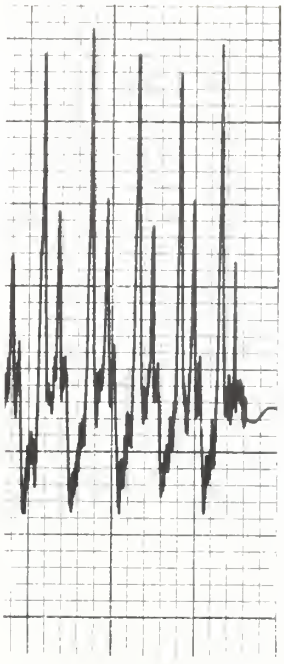

f.

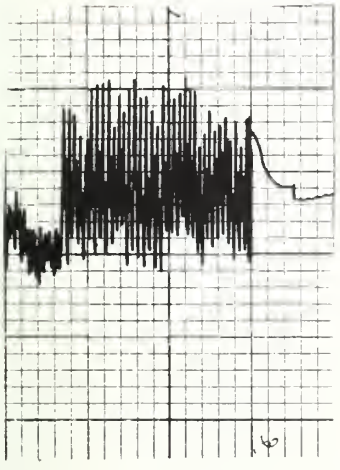

g.

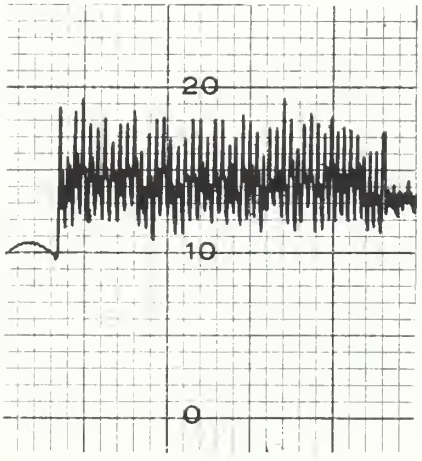

h.

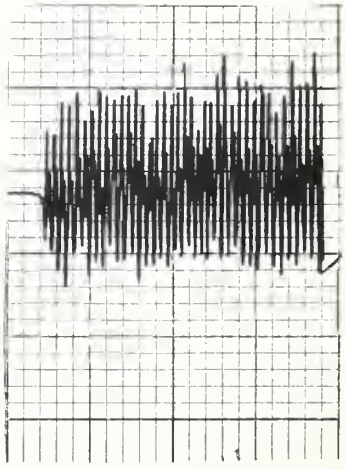

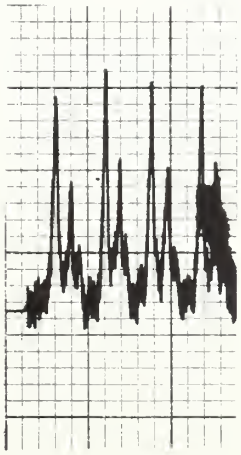

j.

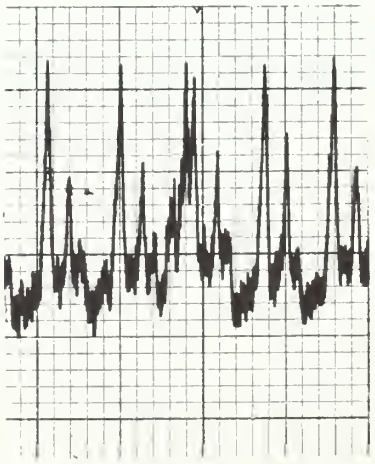

k.

FIGURE XVIII

Effect of Rotation Speed and Time Constant on Counting Rate

Fixed operating conditions: 45 Kv 40 ma.

Beam length approximately 8 millimeters
Beam width approximately 20 mils

Defects: One 40 mil diameter hole in five foils properly aligned, one 40 mil diameter hole in five foils not aligned.

Fig.	Speed (RPM)	Time Constant (seconds)
a.	.7	2
b.	.7	1
c.	1.2	2
d.	1.2	1
e.	1.8	2
f.	1.8	1
g.	16	1
h.	12	2
i.	12	1
j.	1.8	1
k.	1.2	1

Figures j. and k. differ from f. and d. in that the defects are hidden by another foil of zirconium approximately 8 mils thick.

TABLE V

Effect of Rotation Speed and Time Constant on Counting Rate

Figure	High Peak	Low Peak	Minimum	2nd Minimum
a	202-210 cps	180-198	47	72
b	347-360	214-230	40-45	88
c	184-192	166-184	46-53	72
d	306-316	186-205	40-42	72
e	170-182	156-167	49-56	--
f.	256-277	164-195	50	--
g	120-146	--	78-87	--
h	136-167	--	56-72	--
i	128-157	--	68-92	
Fixed Count	351.6	230.5	49.1	94.8

Background 44.6

Fractional Standard Deviation (Fixed Count) = .7%

Counting rates from Figure XVIII.

FIGURE XIX
Defect Peaks for Various Beam Lengths and Widths

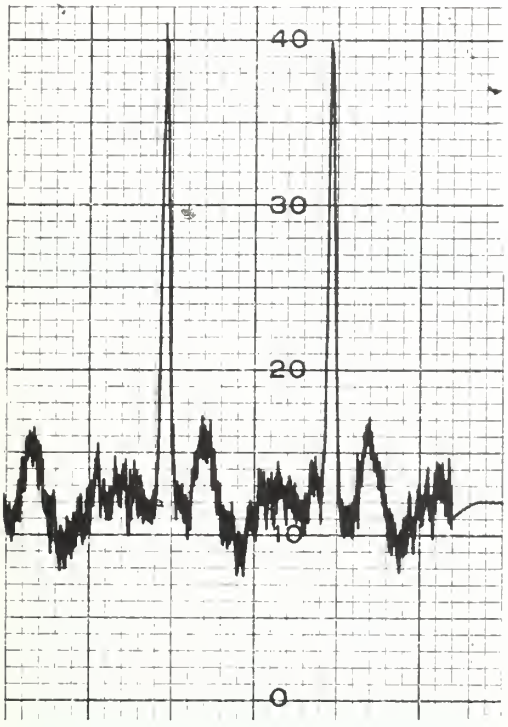

a.

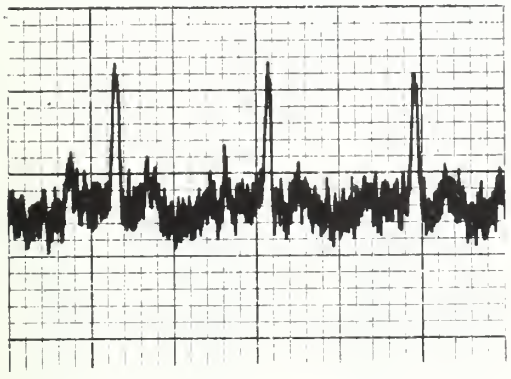

b.

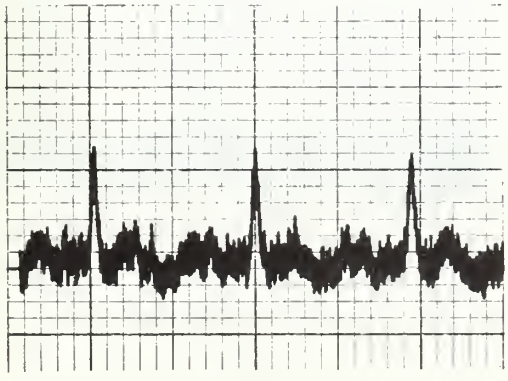

c.

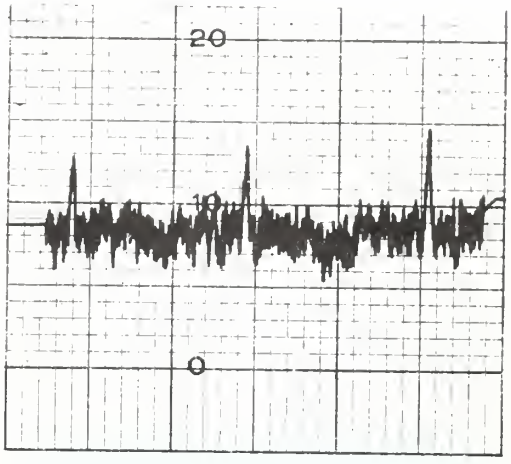

d.

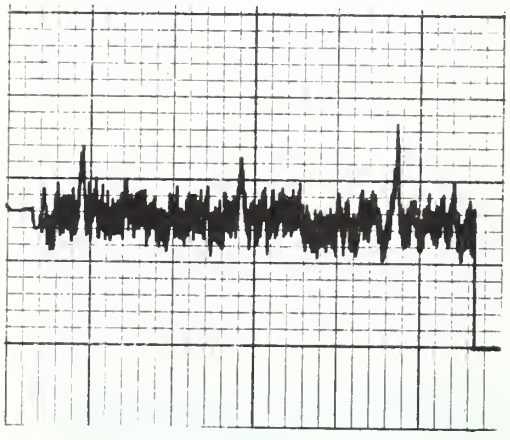

e.

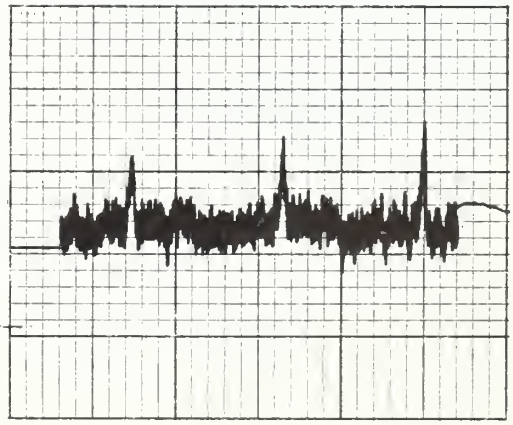

f.

FIGURE XIX

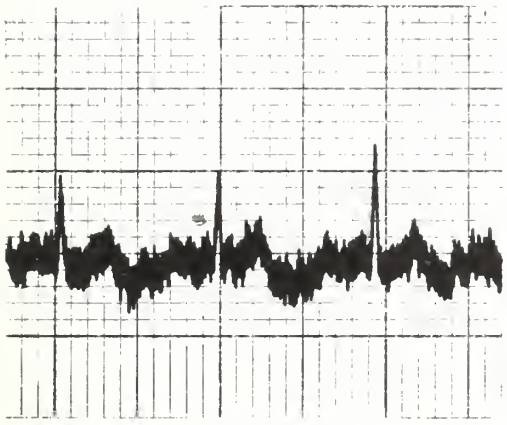

g.

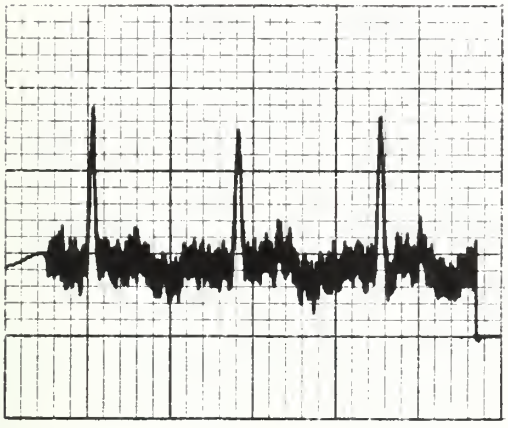

h.

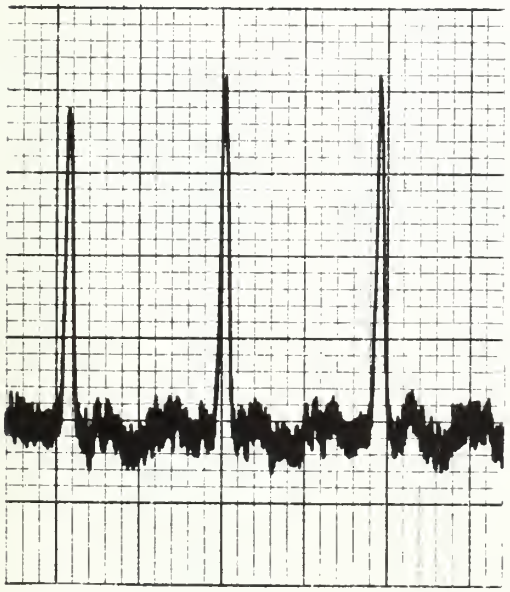

i.

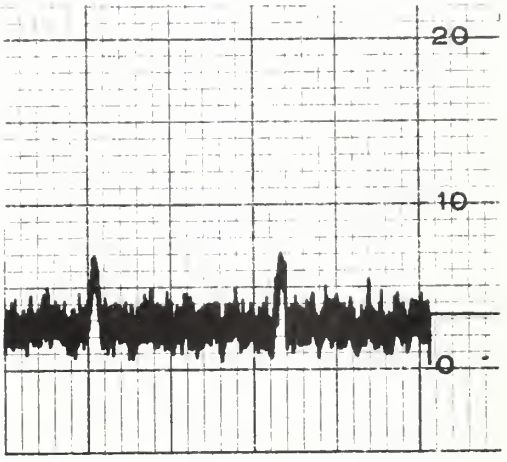

j.

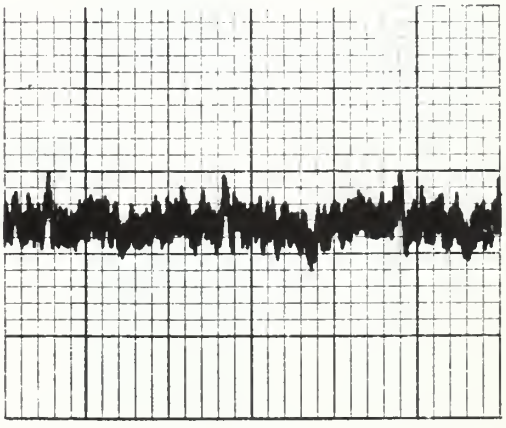

k.

Figure XIX

a.	39 mil defect with slit #2	Beam:	L	=	16.62 W	=	.74
b.	39 mil defect with slit #6		L	=	13.08 W	=	.25
c.	39 mil defect with slit #9		L	=	16.66 W	=	.20
d.	20 mil defect with slit #6		L	=	13.08 W	=	.25
e.	20 mil defect with slit #7		L	=	9.20 W	=	.25
f.	20 mil defect with slit #8		L	=	4.90 W	=	.25
g.	13.5 mil defect with slit #4		L	=	5.02 W	=	.74
h.	20 mil defect with slit #4		L	=	5.02 W	=	.74
i.	39 mil defect with slit #4		L	=	5.02 W	=	.74
j.	39 mil defect with slit #5		L	=	14.50 W	~	.08
k.	13.5 mil defect with slit #8		L	=	4.90 W	=	.25

All recordings taken as follows:

Time constant = 1 second

Speed = .7 revolutions per minute

Scale factor = 8 cps/division

Tube voltage = 45 kilovolts

Tube current = 40 milliamperes

Slit # 6 at Pin

Slit # 7

Slit # 8

Slit # 9

Slit # 10

Slit # 2

Slit # 3

Slit # 4

Slit # 5

Slit # 6 at Collimator

FIGURE XX
Slit Sizes

TABLE VI

Computed versus Actual Counting Rates for Defects Using Various Beam Sizes

Slit No.	Beam Area sq. mm.	Bare Pin cps/sq. mm.	Normal Pin cps
1	5.90	331	50
2	12.30	327	84
3	5.92	404	54
4	3.71	395	39
6	3.33	363	61
7	2.57	366	58
8	1.37	417	50
9	3.33	269	26
10	1.56	345	21

Slit No.	13.5 mil defect			20 mil defect			39 mil defect		
	Area	Comp.	Act	Area	Comp.	Act	Area.	Comp.	Act
1	.093	81	90	.203	116	111	.500	218	218
2	.093	114	127	.203	150	163	.658	298	300
3	.093	96	92	.203	140	132	.658	324	274
4	.093	75	79	.203	118	108	.658	298	229
6	.084	92	91	.135	110	100	.274	160	131
7	.084	89	63	.135	107	93	.274	157	136
8	.084	85	81	.135	106	93	.274	164	135
9	.062	42	39	.099	52	43	.197	79	76
10	.062	42	28	.099	55	33	.197	89	65

The loss of counts from defect area has been neglected in the computation of expected counting rate. This would reduce the computed counting rates by 2 counts at the most for the 39 mil defect and lesser amounts for the smaller defects.

TABLE VII

Effect on Counting Rate of Location of Defect in Beam

Defect Location	Total Counts	Run 1	Run 2	Run 3	Counts/ Second
Beam center	6400	57.50	57.92	57.60	111.0
4 mm to left	6400	62.82	62.41	61.10	103.4
4 mm to right	6400	62.75	62.75	64.50	100.9
Out of Beam	1600	31.90	31.95	32.15	50.0

Defect size - .51 mm in diameter

Beam length - 8 mm

Beam width - .66 mm

TABLE VIII

Defect Area Required to Give a Fixed Counting Rate Increase for a Given Cladding Thickness and Thickness of Cladding over the Defect

Counting rate from the bare uranium surface - 360 cps/sq. mm.

0 mil of cladding covering the defect

Counting Rate Increase	Defect Area Required for Normal Thickness of			
	6 mils	5 mils	4 mils	3 mils
5 cps	.014 sq. mm.	.014	.014	.015
10	.028	.028	.028	.029
20	.056	.056	.057	.059
30	.084	.084	.085	.088
40	.112	.112	.114	.118
50	.140	.140	.142	.147

1 mil of cladding covering the defect

5	.040	.041	.043	.048
10	.081	.083	.086	.096
20	.162	.165	.173	.192
30	.243	.248	.259	.289
40	.324	.331	.345	.385
50	.410	.413	.431	.481

2 mils of cladding covering the defect

5	.104	.109	.123	.174
10	.209	.219	.246	.348
20	.417	.437	.592	.696
30	.626	.656	.738	1.045
40	.835	.875	.984	1.394
50	1.043	1.094	1.230	1.742

TABLE VIII (cont.)

3 mils of cladding covering the defect

Counting Rate Increase	Defect Area Required for Normal Thickness of 6 mils	5 mils	4 mils
5 cps	.260 sq. mm	.294	.418
10	.520	.587	.837
20	1.040	1.174	1.674
30	1.560	1.762	2.510
40	2.080	2.349	3.347
50	2.600	2.936	4.184

For other intensities, multiply the areas above by the ratio of 360 to the new intensity.

TABLE IX

Expected Counting Rates for a Given Cladding Thickness and Beam Area

Beam Area	Normal Cladding Thickness 6 mils	5 mils	4 mils	3 mils
.50	.88 cps	1.98	4.52	10.49
1.00	1.76	3.96	9.04	20.98
2.50	4.41	9.90	22.59	52.40

DISCUSSION

The problem of finding cladding defects in small diameter, zircalloy clad reactor fuel pins is an important one in industry today. It has not been successfully solved and yet reactors utilizing this type of pin are in various stages of design and construction. The fuel pin (fig.XII) used in this study is a prototype obtained from Nuclear Metals, Inc. The problem is to devise a method for complete inspection of the cladding of each pin, in a short time, with assurance that all defects that could cause failure of the pin when it is in use have been found. Fluorescent x-ray techniques appeared to offer a possible solution to the problem.

After a preliminary investigation to study some of the equipment design parameters, plans were drawn and the equipment manufactured. The cladding defect detector performed quite successfully in the measurement of cladding thickness utilizing a static scan. After this preliminary work, studies were begun on locating cladding defects. The problem immediately arose as to how suitable defects could be made which could be measured and were reproducible. It was felt that small circular defects would represent the worst condition with the exception of a crack around the circumference. This latter type of defect does not seem too likely in an extruded pin. The cladding could be filed down, but this method was not easily reproducible nor susceptible to measurement. Indentations made with a Rockwell hardness tester were easily reproduced but could not be measured easily. The wrapping of layers of foil around a bare portion of the pin seemed to be a good method. Holes could be drilled in individual foils and thus defects with thicknesses of cladding above the defect could be simulated. In this way defects of known size, and which were reproducible would be available.

Unfortunately, the difficulty in insuring the alignment of the defect in the various foils was considerable. Attempts to drill holes with the foils already around the pin were unsuccessful due to the drill bending and thus tending to rip and tear the foils rather than drilling a smooth hole. It was finally decided that drilling holes of various diameters in the cladding would be the best as far as known size and reproducibility were concerned.

It was desirable that background be reduced to a minimum. One of the methods used was to have an opening at the detector which was only as large as necessary to admit the focused line, but which would not allow any other radiation to enter and be counted. The original detector window was .375" wide. A photograph taken at the window revealed a sharp, narrow line with some spread of intensity. This narrow line appeared to be about 10 mils wide. A slit 25 mils wide then was installed and the intensities compared. Fixed count time measurements revealed an increase in defect peak to background of two to one. (TableIV). Unfortunately, this reduced the peak intensity such that the defect as shown on the recorder charts do not stand out anywhere near as clear. (fig.XVII) This is partly due to statistical and other fluctuations becoming relatively more important. However, the major difference is that background and the defect are not the only contributors to the counting rate. The rest of the effective slit area, in addition to the defect area, contributes to the counting rate, this contribution being considerable when small defects are involved.

The final result of the investigation was that a 50 mil slit was used as the detector window. The length was such as to permit the full scintillation crystal to be effective for detection. Better photographs showed

that the width of the beam entering the detector was approximately 25 to 30 mils in width. The additional width was used to avoid difficulties in adjusting the slit to give a maximum peak to background counting rate.

With other conditions fixed, the effect of pin rotation speed on defect location is shown in fig. XVIII. There are two holes approximately 40 mils in diameter in a simulated cladding, consisting of about 4 mils of zirconium foil wrapped around a bare section of the pin, which are causing the peaks. There is a section of the simulated cladding where the thickness is about 7 mils. The difference in height of the two peaks is the result of not being able to align properly both defects in the foils.

As a result of typical scans like this, it was found that the detection of defects by this equipment was severely limited by the recording equipment. The Brown recorder has a maximum chart speed of 1/2 inch per minute. This compresses several rotational scans of the pin into only 1/2 inch of the chart. This was not too serious if the rotation speed was not very fast, as the maximum and minimum counting rate was still shown.

A more serious limitation was the inability of the equipment to record an accurate counting rate with good precision. Table V compiles counting rates for the defect plots shown in fig. XVIII and from fixed count time measurements.

Disregarding the runs at 12 and 16 rpm, there is still a considerable spread of counting rates in the scans. As speed of rotation increases, the recorded counting rate falls off. This is a result of the counting rate meter integrating the defect counts over a larger area and the inability of the recording pen to respond instantaneously. The effect of the time constant can easily be seen. Decreasing the time constant reduces the integration time rather markedly. (fig. XVIII). A one second time

constant was the minimum available with this equipment. These restrictions, imposed by the recording equipment, effectively limited the maximum pin rotation speed that could be used during the investigation.

The effect of beam size, as fixed by the collimator slit length and width, was investigated. It was found that essentially the same counting rate per square millimeter was given off independent of beam size. Table VI shows the actual and computed counting rates from the defects with various beam sizes. A count was taken from the bare section to determine the counting rate per unit area. The defects were drilled through to the meat and as the area of the defect was known, the counting rate it should give was computed. To this was added the counting rate obtained from a normal section of the pin. These computed rates compared favorably with the actual. The difference is due mainly to two effects. One was the inability to get the beam area exactly. The other was the failure to account for a small loss due to the defect beam having to pass through part of the cladding, rather than being able to come straight out of the hole and avoid being attenuated. Since the crystal used to separate the pure wavelength was only .6 inches wide, no beams longer than this were usable. This accounts for the low counting rate per unit area received from the slit that was about .7 inches long. Relative slit sizes and their ability to locate defects are shown in fig. XIX

The choice of collimator slit length and width (and thus beam length and width) is very important. A long length enables faster inspection of each rod, since for a given rotation speed, the longer length permits faster translation of the rod through the beam. Or conversely, it permits slower rotation of the pin for a fixed inspection time. For defect

location, a short length is desirable. For a given defect, the short length would effectively give the highest percentage change in counting rate as compared to the counting rate without the defect. A width of beam equal to or less than the average expected width of a defect would be desirable.

Thus, some type of compromise must be made between the short length and the long length. For a given counting rate increase and initial cladding thickness, TableVIIIshows the minimum defect area when covered with another given thickness of cladding, which can be detected. The intensity used in the computation is 360 cps per square millimeter, which is the average intensity attained from the bare pin surface with the experimental equipment. Other intensities may be used by multiplying with the appropriate constant.

It has been assumed for purpose of constructing the table that equipment can be constructed which could detect increases in counting rates as low as 5 cps. Table IX shows the counting rates that would be received with the given beam area and thickness of cladding. From surveying these two Tables, it is immediately apparent as to what the major problem with this type of inspection is. For the 360 cps intensity, a decrease in the cladding of 6 mils to 5 mils, for a 2.50 square millimeter beam area, would have the same effect as a defect area of .26 square millimeters covered with 3 mils of claddings, or a .040 square millimeter defect with 1 mil of cladding cover. There would be no way of telling whether it was a decrease in cladding thickness which was causing this increase or whether it was a defect. It is likely that the .040 square millimeter defect would be cause for rejection, while the decrease in cladding thickness or the .26 square millimeter defect would not be enough for

rejection. The long slit would be unable to resolve which was the cause, but a spot beam could be used to measure the cladding thickness in a small area and thus determine if the thickness was too small. Using the tables, any combination of defect size and coating can be matched to an equivalent decrease in cladding thickness.

Fortunately, the extrusion process makes the possibility of there being small, pinhole types of defects in these pins rather small. The expected defect is that caused by a hard grain not being completely compressed, but smeared out into a small bump extending along the pin and into the cladding. The thickness of cladding over this hard grain would vary. These bumps may be about 20 mils in width and 1/4" to 1/2" in length. Thus they would permit the use of a fairly large beam size, both in length and width.

Assuming this type of defect, the following inspection pattern could be followed. The equipment could be set to mark any area on the pin that gave a counting rate equivalent to 3.5 mils of cladding thickness, for example, if the minimum thickness allowed was 3 mils. Then these areas could be checked with a much smaller, essentially spot beam to determine if the cladding was less than the minimum thickness allowed at any point.

The use of this process for inspection should be feasible if the defects are as stated above. Detection equipment should be designed so that rotation speeds of 10 or more rpm would be feasible depending on the intensity. Using a beam 12mm long with a 4 mm overlap on each rotation, each pin could be inspected in about 10 minutes. Time required for inspection of all pins would still be rather large but not unreasonable. Sectioning and inspection of several of these pins is required to determine exactly what types of defects can be expected.

The results of the study show that this method will work in detecting cladding defects. It has also shown where improvements in the equipment design can be made which would enable smaller defects to be located and which would speed up the inspection of a pin.

A method of rotating and translating a pin through the beam at the same time will be required. The particular method used should not be critical as long as the same geometry is maintained. It had been the intention to inspect some pins as a final step in the study. Due to the limitations of the recording equipment, the rotation-translation equipment was not built. There should be no problems associated with both rotation and translation as long as the translation per rotation is about 75% of the beam length.

Substantial gains in intensity should be obtained by decreasing the distance the beam must travel from the x-ray tube to the detector. There will be two limiting factors in reducing this distance. One is the size of the x-ray tube which limits how close the pin can be to the tube to reduce $1/r^2$ losses and still permit as close to 180 degree takeoff angle as possible. If the incoming beam and outgoing beam do not travel normal to the pin, intensity is lost from attenuation by the cladding due to the longer path length through the cladding.

The second limitation is the radius to which the crystal can be bent. As the path length from pin to crystal to detector is shortened, the crystal must be bent to a smaller radius. There is a minimum radius beyond which the crystal cannot be bent without breaking. These limitations effectively limit the gain in intensity attainable by reducing path length. A slight improvement might also be possible with a different crystal.

Improving detection efficiency will result in effective gains in intensity. The use of a doubly bent crystal should result in better efficiency. This would include the intensity now being lost because of the limited width of the scintillation detector crystal. The doubly bent crystal would reduce the spread of the beam from the pin and could also help in reducing background by reducing the length of the required window. If the doubly bent crystal should not prove feasible, increasing the size of the bent crystal and of the scintillation detector crystal would both aid in effectively increasing the intensity.

Improved collimator design should result in increased intensity. The present design limits the area of the x-ray source that contributes to the beam intensity. By study and proper design, it should be possible to use more of the x-ray source in contributing to the incoming intensity.

The area which will need the most study and work is the recording equipment. Fast reacting equipment will be needed if suitable rotation speeds are to be used. A shorter time constant will be needed to permit the equipment to respond to the changes in counting rate. Faster rotation of the pin means, for a fixed time constant, that the detected counts are being integrated over a larger pin area and thus tending to wash out any variation in counting rate. A smaller time constant also means that statistical variations become more important and would tend to hide changes in the measured counting rate. By increasing the intensity, the statistical fluctuations would be reduced. The final recording equipment used will probably have to be electronic to permit the fast recording times desired.

CONCLUSIONS

The following conclusions have been reached by the authors based on the results of this study:

1. The cladding thickness of small diameter, thin cladding fuel pins can be measured accurately up to thicknesses of about 7 mils with the equipment available. A 5% change in intensity at 5 mils cladding is equivalent to .06 mils.

2. Defects in the cladding can be found in a continuous scanning process. The commercial use of this equipment for quality control and inspection of all fuel pins of the type used in this study, i.e., zircalloy clad pins with a nominal cladding thickness of 5 to 6 mils, will depend on the standards that are set. Standards can be set using the tables included herein.

3. The primary difficulty will be in trying to distinguish between a cladding defect and a small reduction in overall cladding thickness. The pin may be good if the latter case is true, whereas a small hole in the cladding would call for rejection of the pin.

4. Better detection and recording equipment will be required if the inspection is to be fast enough to permit the complete inspection in a reasonable time of all of the pins required for a reactor core loading.

RECOMMENDATIONS

Based on the results of the investigations carried out, the following recommendations are made:

1. That better and faster acting detection equipment be designed to permit faster rotation of the pin.

2. That a study be made of the equipment design to increase the intensity of the detected beam. Among items to be studied are closer location of pin to tube, crystal to detector, and detector to crystal, and collimator design.

3. That a doubly bent crystal be used to obtain more intensity. If this is not feasible, then a larger scintillation crystal be used to permit full detection of the beam.

4. That suitable equipment be designed to permit total inspection of the pin by means of simultaneous rotation and translation of the beam.

5. That typical production pins be sectioned to determine the normal type of defect to be expected and what variation in cladding thickness can normally be expected.

APPENDIX

APPENDIX A

SUPPLEMENTARY DISCUSSION

The mass absorption coefficient of zirconium was obtained utilizing an x-ray spectrometer with a lithium fluoride crystal. This was a standard table top unit, consisting of the x-ray source, specimen, crystal and collimator, made by Norelco. The detection device used in the investigation consisted of a thallium activated sodium iodide crystal scintillation counter. This is a package unit consisting of the scintillation crystal, photomultiplier tube and preamplifier made by Norelco. A Soller collimator acted to collimate the beam of fluorescent radiation from the specimen. The recording equipment utilized throughout the study consisted of a scintillation/proportional unit, Norelco 42234, and electronic circuit panel, Norelco 12048. The scintillation/proportional unit contained a linear pulse amplifier, amplitude discriminator, and high speed binary counting stages. The binary stages were not used because of their erratic operation. The electronic control panel contained a Brown recorder, clock and interval timer, DC power supply, and electronic voltage stabilizer.

To determine the thickness of the different sets of foils, a large sheet of each foil thickness was carefully weighed on a chemical balance and its area was measured. The mass/unit area could be determined from this. By using an average value of density of 6.46 grams/cubic centimeter, the thickness could be determined accurately. For experimental purposes, the foil was cut into smaller sections.

During the course of the investigation, some trouble was caused by interference from outside sources. Three distinct sources of trouble

which gave false counting rates were:

1. Induction furnace
2. Radar
3. Local power supply variations

These interferences caused the recorder to give false peaks which might possibly be mistaken for defects. The first two sources in general were so strong that it was obvious that the peak was due to interference. The third source was harder to detect because of its lesser strength. All three caused difficulties when fixed count time measurements were being made, but were detectible normally because of the change in the trend of previous counting rates.

APPENDIX B

TABLE X

Measurement of cladding thickness

Foil Thickness - .862 mils

No. Foils	Total Counts	Run 1	Run 2	Run 3
0	12800	9.89	9.65	9.65
1	12800	21.00	21.23	21.25
2	6400	21.43	21.55	21.60
3	6400	29.90	29.60	29.30
4	6400	51.20	50.95	51.60
5	6400	78.50	76.43	76.45
6	6400	100.69	102.63	101.54
7	6400	114.00	110.60	111.32

Foil Thickness - .941 mils

0	12800	6.00	6.05	6.02
1	12800	16.30	15.95	16.08
3	6400	34.40	33.85	34.40
5	6400	85.83	84.40	85.10
6	6400	109.90	111.90	111.30

Foil Thickness - 2.470

0	12800	6.02	6.00	6.05
1	6400	28.12	28.12	27.55
2	6400	95.10	90.40	93.29

TABLE XI

Counting rates from different defects using various beam sizes

X-ray unit 45 kv - 40 ma Dynode voltage - 1000 volts

Slit	Type	Total Counts	Run 1	Run 2	Run 3
1	Bare	12800	6.38 sec.	6.50	6.52
	Normal	1600	31.9	32.3	31.8
	13.5	6400	71.69	71.72	70.43
	20	6400	57.50	57.60	57.92
	39	6400	29.28	29.15	29.00
2	Bare	25600	6.30	6.30	6.36
	Normal	1600	18.52	19.30	19.38
	13.5	3200	25.62	25.51	24.20
	20	3200	19.65	19.60	19.64
	39	6400	21.24	21.40	21.45
3	Bare	25600	10.59	10.52	10.60
	Normal	1600	27.66	27.86	27.64
	13.5	1600	17.03	17.49	17.59
	20	3200	24.45	23.71	24.68
	39	3200	11.90	11.64	11.48
4	Bare	25600	8.62	8.52	8.56
	Normal	1600	41.49	41.02	40.50
	13.5	1600	20.75	20.10	20.25
	20	1600	14.89	14.52	15.08
	39	3200	13.80	13.95	14.20

TABLE XI(cont.)

X-ray unit 45 kv - 40 ma Dynode voltage - 1000 volts

Slit	Type	Total Counts	Run 1	Run 2	Run 3
6	Bare	12800	10.35 sec.	10.45	10.21
	Normal	3200	51.70	52.85	52.55
	13.5	1600	18.10	17.68	17.21
	20	3200	31.71	32.01	31.85
	39	3200	24.08	24.38	24.60
7	Bare	12800	13.40	13.10	13.00
	Normal	1600	28.40	27.42	27.42
	13.5	1600	25.70	26.00	24.40
	20	1600	16.90	17.25	17.28
	39	3200	23.05	23.90	23.52
8	Bare	12800	21.48	21.20	21.14
	Normal	1600	31.55	32.40	31.70
	13.5	1600	19.40	20.19	19.60
	20	1600	16.85	17.56	17.15
	39	1600	11.78	11.95	11.90
9	Bare	12800	13.90	13.86	13.62
	Normal	1600	59.80	62.10	60.56
	13.5	1600	41.12	41.20	40.90
	20	1600	37.50	37.51	36.10
	39	1600	20.90	20.82	21.50
10	Bare	12800	22.48	22.40	22.43
	Normal	800	35.08	38.45	39.60
	13.5	800	28.78	29.80	27.80
	20	800	24.75	24.20	23.56
	39	1600	25.45	24.43	24.53

APPENDIX C

SAMPLE CALCULATIONS

1. Calculation of expected counting rate with defect in beam (Table VI)

$C_t = (A_d)(C_b) + C_n$

$= (.0928)(327) + 84$

$C_t = 114$ counts/second

C_t = total counting rate with defect in beam in cps

C_b = Bare uranium counting rate in cps/sq. mm.

C_n = Counting rate from normal cladding in cps

A_d = Area of defect in sq. mm.

2. Calculation of defect area with a certain covering of cladding to give a counting rate increase with a given initial thickness of cladding

$$A_d = \frac{X}{C_b (R_d - R_t)}$$

$$= \frac{5}{360 (1 - .00490)}$$

$A_d = .014$ square millimeters

A_d = Defect area in sq. mm.

C_b = Bare counting rate in cps/sq. mm.

R_d = Normalized counting rate for assumed thickness over defect

R_t = Normalized counting rate for initial cladding thickness

X = Counting rate increase in cps

3. Calculation of expected counting rate from pin with normal cladding thickness and given area

$C_n = A_b C_b R_t$

$= (.50)(360)(.00490)$

$C_n = .881$

C_n = Counting rate from normal cladding in cps

A_b = Area of beam in sq. mm.

C_b = Bare pin counting rate in cps/sq. mm.

R_t = Normalized counting rate for normal cladding thickness

4. Calculation of defect area in beam

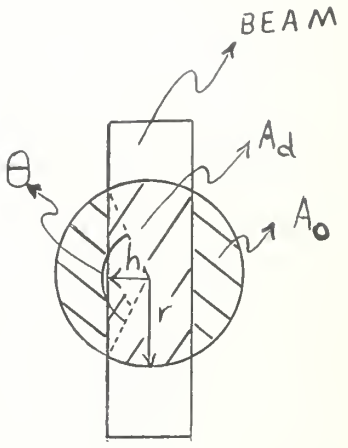

$A_t = r^2 \pi$

$= (3.14)(.495)^2$

$A_t = .772$ square millimeters

$\theta = 2 \cos^{-1} h/r$

$= 2 \cos^{-1} .14/.495$

$\theta = 147.2$ degrees

$A_o = r^2 (\theta - \sin \theta)$

$= (.495)^2 \left(\frac{147.2}{180} - \sin 147.2\right)$

$A_o = .498$

$A_d = A_t - A_o$

$= .772 - .498$

$A_d = .274$ square millimeters

A_t = total area of defect in square millimeters

r = radius of defect in millimeters

A_o = defect area outside beam in square millimeters

θ = angle of sector outside beam in degrees

A_d = defect area in beam

h = half width of beam in millimeters

LIST OF REFERENCES

1. B. J. Lowe and P. D. Sierer, "Cladding Thickness of Fuel Elements by X-Rays", Thesis, MIT, (May 1958), pp 28-45.

2. C. S. Barret, Structure of Metals, McGraw-Hill Book Co., New York, (1952), pp 45-64.

3. R. D. Evans, The Atomic Nucleus, McGraw-Hill Book Co., New York, (1955).

4. Nondestructive Tests in the Field of Nuclear Energy, ASTM Special Technical Publication #223, Philadelphia, (1958).

5. A. Guinier, X-Ray Crystallographic Technology, Hilger and Walls, London (1952), pp 160-174.

6. A. H. Compton and S. K. Allison, X-Rays in Theory and Experiment, D. Van Nostrand Co., New York (1949).